Delay stabilization of rotating waves near fold bifurcation and application to all-optical control of a semiconductor laser

B. Fiedler,[1] S. Yanchuk,[2,3] V. Flunkert,[4] P. Hövel,[4] H.-J. Wünsche,[5] and E. Schöll[4]
[1]*Institut für Mathematik I, FU Berlin, Arnimallee 2-6, D-14195 Berlin, Germany*
[2]*Weierstraß Institut für Angewandte Analysis and Stochastik, Mohrenstraße 39, D-10117 Berlin, Germany*
[3]*Humboldt Universität zu Berlin, Institut für Mathematik, Rudower Chaussee 25, D-12489 Berlin, Germany*
[4]*Institut für Theoretische Physik, Technische Universität Berlin, Hardenbergstraße 36, D-10623 Berlin, Germany*
[5]*Humboldt Universität zu Berlin, Institut für Physik, Newtonstrße 15, D-12489 Berlin, Germany*
(Received 18 February 2008; published 10 June 2008)

We consider the delayed feedback control method for stabilization of unstable rotating waves near a fold bifurcation. Theoretical analysis of a generic model and numerical bifurcation analysis of the rate-equations model demonstrate that such orbits can always be stabilized by a proper choice of control parameters. Our paper confirms the recently discovered invalidity of the so-called "odd-number limitation" of delayed feedback control. Previous results have been restricted to the vicinity of a subcritical Hopf bifurcation. We now refute such a limitation for rotating waves near a fold bifurcation. We include an application to all-optical realization of the control in three-section semiconductor lasers.

DOI: 10.1103/PhysRevE.77.066207 PACS number(s): 05.45.Gg, 02.30.Ks, 42.55.Px, 02.30.Oz

I. INTRODUCTION

Control of complex irregular dynamics is one of the central issues in applied nonlinear science [1]. Starting with the work of Ott, Grebogi, and Yorke [2], a variety of methods have been developed in order to stabilize unstable periodic orbits (UPOs) embedded in a chaotic attractor by employing tiny control forces. A particularly simple and efficient scheme is time-delayed feedback control as suggested by Pyragas [3]. In recent years the notion of *chaos control* has been extended to a much wider class of problems involving the stabilization of unstable periodic states in nonlinear dynamic systems, and has been applied to a vast range of problems in physics, chemistry, biology, medicine, and engineering. However, a deepened understanding of the control schemes and analytic insight into their potential limitations is still a challenging task.

Recently, Fiedler *et al.* [4] have refuted an often invoked assertion, the so-called "odd-number limitation" of delayed feedback control. This purported limitation claims that a periodic orbit with an odd number of real Floquet multipliers greater than unity cannot be stabilized by the time-delayed feedback control in the form proposed by Pyragas [3]. The papers [4–6] show the possibility of stabilization of unstable periodic orbits, which are generated by a subcritical Hopf bifurcation. In our paper, we consider the case when the unstable periodic orbit is generated by a fold bifurcation of saddle-node type [see Eq. (1) below]. We show that such orbits can be stabilized by delayed feedback control. We will restrict our analysis to the case when the periodic orbits have the special form of rotating waves. This case is particularly important for applications to optical systems and, in addition, allows detailed analytical treatment. One such system, a three-section semiconductor laser, will be considered in our paper. Numerical bifurcation analysis confirms that an all-optical delayed feedback control can successfully stabilize rotating waves close to a fold bifurcation in this system. All-optical control exploits the advantage of delayed feedback control, as well as simplicity and inherent high-speed operation. All-optical control of unstable steady states close to a supercritical Hopf bifurcation of the same system has been reported in Ref. [7].

The plan of our paper is as follows: Sec. II is devoted to the analytical treatment of a generic model for fold bifurcations of rotating waves. We derive necessary and sufficient conditions for successful control. In particular, we show that the stabilization can be achieved by delayed feedback with arbitrarily small control amplitude provided the phase of the control is chosen appropriately. In Sec. III, we study a rate-equation model for three-section semiconductor lasers with all-optical delayed feedback. For suitably chosen parameter values, this model has a fold bifurcation. Numerical bifurcation analysis establishes successful control in the vicinity of this bifurcation.

II. ANALYSIS OF FOLDS OF ROTATING WAVES

A. Properties of the fold system without control

As a paradigm for fold bifurcation of rotating waves we consider planar systems of the form

$$\dot{z} = g(\lambda, |z|^2)z + ih(\lambda, |z|^2)z. \tag{1}$$

Here $z(t)$ is a scalar complex variable, g and h are real valued functions, and λ is a real parameter. Systems of the form (1) are S^1-equivariant, i.e., $e^{i\theta}z(t)$ is a solution whenever $z(t)$ is, for any fixed $e^{i\theta}$ in the unit circle S^1. In polar coordinates $z=re^{i\varphi}$ this manifests itself by the absence of φ from the right-hand sides of the resulting differential equations

$$\dot{r} = g(\lambda, r^2)r,$$

$$\dot{\varphi} = h(\lambda, r^2). \tag{2}$$

In particular, all periodic solutions of Eq. (1) are indeed rotating waves, alias harmonic, of the form

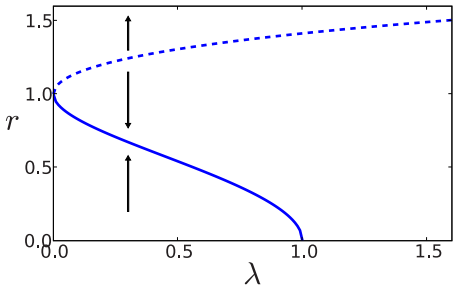

FIG. 1. (Color online) Bifurcation diagram of rotating waves (solid line: stable; dashed line: unstable) of Eqs. (1) and (4). Arrows indicate (in)stability according to Eq. (2).

$$z(t) = re^{i\omega t}$$

for suitable nonzero real constants r, ω. Specifically, this requires $\dot{r}=0$, $\dot{\varphi}=\omega$

$$0 = g(\lambda, r^2),$$

$$\omega = h(\lambda, r^2). \tag{3}$$

Fold bifurcations of rotating waves are generated by the nonlinearities

$$g(\lambda, r^2) = (r^2 - 1)^2 - \lambda,$$

$$h(\lambda, r^2) = \gamma(r^2 - 1) + \omega_0. \tag{4}$$

Our choice of nonlinearities is generic in the sense that $g(\lambda, r^2)$ is the normal form for a nondegenerate fold bifurcation [8] at $r^2=1$ and $\lambda=0$ (see Fig. 1 for the resulting bifurcation diagram). We fix coefficients $\gamma, \omega_0 > 0$.

Using Eqs. (3) and (4), the amplitude r and frequency ω of the rotating waves then satisfy

$$r^2 = 1 \pm \sqrt{\lambda}, \quad \omega = \omega_0 + \gamma(r^2 - 1) = \omega_0 \pm \gamma\sqrt{\lambda}. \tag{5}$$

The signs $\pm$ correspond to different branches in Fig. 1: +, unstable and −, stable.

B. Fold system with delayed feedback control

Our goal is to investigate delay stabilization of the fold system (1) by the delayed feedback term

$$\dot{z} = f(\lambda, |z|^2)z + b_0 e^{i\beta}[z(t-\tau) - z(t)], \tag{6}$$

with real positive control amplitude b_0, delay τ, and real control phase β. Here we have used the abbreviation $f=g+ih$. The Pyragas choice requires the delay τ to be an integer multiple k of the minimum period T of the periodic solution to be stabilized,

$$\tau = kT. \tag{7}$$

This choice guarantees that periodic orbits of the original system (1) with period T are reproduced exactly and noninvasively by the control system (6). The minimum period T of a rotating wave $z=re^{i\omega t}$ is given explicitly by $T=2\pi/\omega$. Using Eqs. (5), Eq. (7) becomes

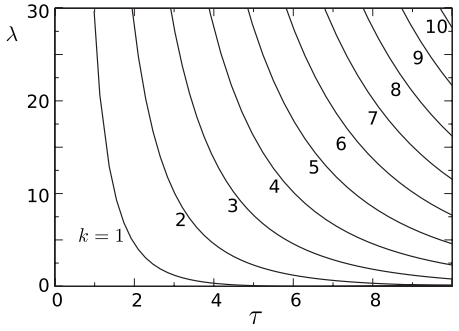

FIG. 2. The Pyragas curves $\lambda=\lambda(\tau)$, corresponding to the unstable branch in Fig. 1, in the parameter plane (τ,λ); see Eq. (9). Parameters: $\gamma=\omega_0=1$.

$$\tau = \frac{2\pi k}{\omega_0 \pm \gamma\sqrt{\lambda}}, \tag{8}$$

or, equivalently,

$$\lambda = \lambda(\tau) = \left(\frac{2\pi k - \omega_0\tau}{\gamma\tau}\right)^2. \tag{9}$$

In the following we select only the branch of $\lambda(\tau)$ corresponding to the τ value with the + sign, which is associated with the unstable orbit. Condition (9) then determines the kth *Pyragas curve* in parameter space (τ,λ), where the delayed feedback is noninvasive, indeed. The fold parameter $\lambda=0$ corresponds to $\tau=2\pi k/\omega_0$, along the kth Pyragas curve [see Fig. 2 for the Pyragas curves in the parameter plane (τ,λ)].

For the delay stabilization system (6) we now consider τ as the relevant bifurcation parameter. We restrict our study of Eq. (6) to $\lambda=\lambda(\tau)$ given by the Pyragas curve (9), because $\tau=kT$ is the primary condition for noninvasive delayed feedback control.

We begin with the trivial case $b_0=0$ of vanishing control, somewhat pedantically; see Sec. II A. For each $\lambda=\lambda(\tau)$, we encounter two rotating waves given by

$$r^2 = 1 \pm \frac{2\pi k - \omega_0\tau}{\gamma\tau}, \quad \omega = \omega_0 \pm \left(\frac{2\pi k - \omega_0\tau}{\tau}\right). \tag{10}$$

The two resulting branches form a transcritical bifurcation at $\tau=2\pi k/\omega_0$. At this stage, the transcriticality looks like an artifact, spuriously caused by our choice of the Pyragas curve $\lambda=\lambda(\tau)$. Note, however, that only one of the two crossing branches features minimum period T such that the Pyragas condition $\tau=kT$ holds. This happens along the branch

$$r^2 = 1 + \frac{2\pi k - \omega_0\tau}{\gamma\tau}, \quad \omega = 2\pi k/\tau$$

(see Fig. 3). We call this branch, which corresponds to "+" in Eq. (10), the *Pyragas branch*. The other branch has minimum period T with

$$kT = \frac{\pi k}{\omega_0\tau - \pi k}\tau \neq \tau,$$

except at the crossing point $\omega_0\tau=2\pi k$. The minus branch therefore violates the Pyragas condition for noninvasive con-

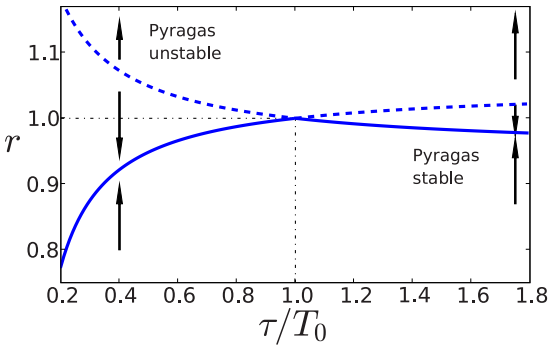

FIG. 3. (Color online) Bifurcation diagram of rotating waves of Eq. (6) at vanishing control amplitude $b_0=0$. Parameters: $T_0=2\pi/\omega_0$, $\omega_0=1$, $\gamma=10$.

trol, even though it has admittedly been generated from the same fold bifurcation.

Our strategy for Pyragas control of the unstable part of the Pyragas branch is now simple. For a nonzero control amplitude b_0, the Pyragas branch persists without change, due to the noninvasive property $\tau=kT$ along the Pyragas curve $\lambda=\lambda(\tau)$. The minus branch, however, will be perturbed slightly for small $b_0\neq 0$. If the resulting perturbed transcritical bifurcation

$$\tau=\tau_c \tag{11}$$

moves to the left, i.e., below $2\pi k/\omega_0$, then the stability region of the Pyragas branch has invaded the unstable region of the fold bifurcation. Again this refutes the notorious odd-number limitation of Pyragas control (see Fiedler *et al.* [4], and references therein).

Let $\tau=\tau_c$ denote the transcritical bifurcation point on the Pyragas curve $\lambda=\lambda(\tau)$ [see Eq. (9)]. Let $z(t)=r_c e^{i\omega_c t}$ denote the corresponding rotating wave, and abbreviate $\varepsilon\equiv r_c^2-1$. In Appendix A, we obtain conditions for the transcritical bifurcation in Eq. (6). As a result, the following relations between the control amplitude b_c at the bifurcation and ε,τ_c are shown:

$$b_c=-\varepsilon\frac{\omega_0+\gamma\varepsilon}{k\pi(\gamma\sin\beta+2\varepsilon\cos\beta)}, \tag{12}$$

and

$$b_c=-\frac{2\pi k-\omega_0\tau_c}{\tau_c\left(\frac{1}{2}\gamma^2\tau_c\sin\beta+(2\pi k-\omega_0\tau_c)\cos\beta\right)}. \tag{13}$$

As follows from Eqs. (12) and (13), for small ε, alias for τ_c near $2k\pi/\omega_0$, *the optimal control angle is* $\beta=-\pi/2$ in the limit $\varepsilon\to 0$, and for fixed $k,\omega_0,\gamma,\varepsilon$ this control phase β allows for stabilization with the smallest amplitude $|b_c|$. For $\beta=-\pi/2$ the relations Eqs. (12) and (13) simplify to

$$b_c=\frac{\varepsilon}{k\pi}\left(\frac{\omega_0}{\gamma}+\varepsilon\right), \tag{14}$$

and

$$b_c=\frac{2}{(\gamma\tau_c)^2}(2k\pi-\omega_0\tau_c), \tag{15}$$

respectively. For small $b_0>0$ we also have the expansions

$$\varepsilon=-\left(k\pi\frac{\gamma}{\omega_0}\sin\beta\right)b_0+\cdots, \tag{16}$$

and

$$\tau_c=\frac{2\pi k}{\omega_0}+\left[\frac{1}{2\omega_0}\left(\frac{2k\pi\gamma}{\omega_0}\right)^2\sin\beta\right]b_0+\cdots. \tag{17}$$

for the location of the transcritical bifurcation. In particular, we see that *odd-number delay stabilization* can be achieved by arbitrary small control amplitudes b_0 near the fold for $\gamma>0$ and $\sin\beta<0$. Note that the stability region of the Pyragas curve increases if $\varepsilon=r_c^2-1>0$ (see Fig. 1). For vanishing phase angle of the control, $\beta=0$, in contrast, *delay stabilization* cannot be achieved by arbitrarily small control amplitudes b_0, near the fold in our system (6).

Even far from the fold at $\lambda=0$, $\tau=2k\pi/\omega_0$, the above formulas (12)–(15) hold and indicate a transcritical bifurcation from the (global) Pyragas branch of rotating waves of Eq. (6), along the Pyragas curve $\lambda=\lambda(\tau)$. This follows by analytic continuation. Delay stabilization, however, may fail long before $\tau=\tau_c$ is reached. In fact, nonzero purely imaginary Floquet exponents may arise, which destabilize the Pyragas branch long before $\tau=\tau_c$ is reached. This interesting point remains open.

A more global picture of the orbits involved in the transcritical bifurcation may be obtained by numerical analysis. Rewriting Eq. (6) in polar coordinates $z=re^{i\varphi}$ yields

$$\dot r=[(r^2-1)^2-\lambda]r+b_0\{\cos[\beta+\varphi(t-\tau)-\varphi]\times r(t-\tau)-r\cos\beta\}, \tag{18}$$

$$\dot\varphi=\gamma(r^2-1)+\omega_0+b_0\{\sin[\beta+\varphi(t-\tau)-\varphi]\times r(t-\tau)/r-\sin\beta\}. \tag{19}$$

To find all rotating wave solutions we make the ansatz $r=$const and $\dot\varphi=\omega=$const and obtain

$$0=(r^2-1)^2-\lambda+b_0[\cos(\beta-\omega\tau)-\cos\beta],$$

$$\omega=\gamma(r^2-1)+\omega_0+b_0[\sin(\beta-\omega\tau)-\sin\beta].$$

Eliminating r we find a transcendental equation for ω

$$0=-\gamma^2\lambda+\gamma^2 b_0[\cos(\beta-\omega\tau)-\cos\beta]+(\omega-\omega_0-b_0[\sin(\beta-\omega\tau)-\sin\beta])^2.$$

One can now solve this equation numerically for ω and insert the result into

$$r=\left(\frac{\omega-\omega_0}{\gamma}-\frac{b_0}{\gamma}[\sin(\beta-\omega\tau)-\sin\beta]+1\right)^{1/2}$$

to obtain the allowed radii (discarding imaginary radii).

The orbit which stabilizes the Pyragas branch in the transcritical bifurcation may be the minus branch or another delay-induced orbit which is born in a fold bifurcation, de-

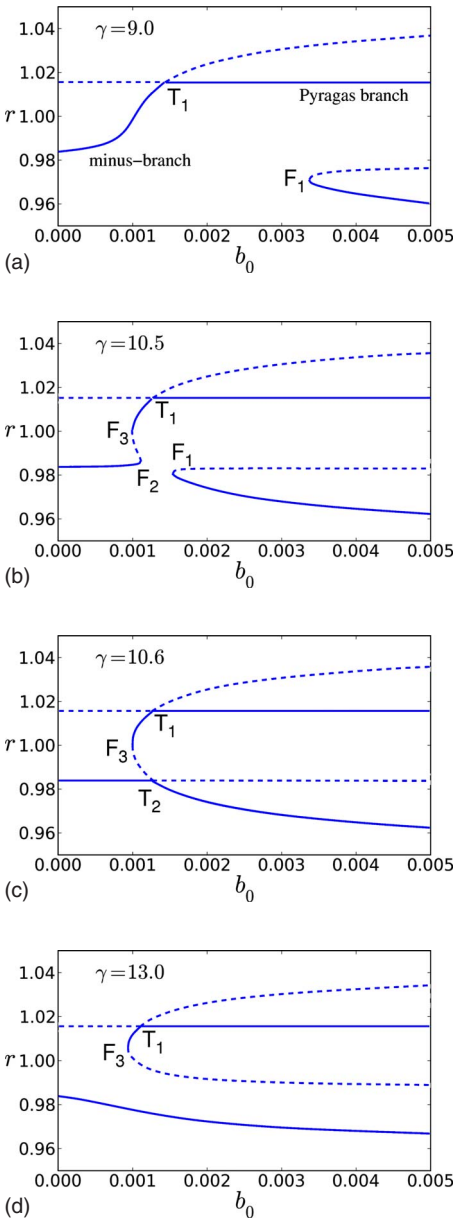

FIG. 4. (Color online) Radii of stable (solid) and unstable (dashed) rotating wave solutions in dependence on b_0 for different γ. Parameters: $\omega_0=1$, $\lambda=0.001$, $\beta=-\pi/2$.

pending on the parameters. Figure 4 displays the different scenarios and the crossover in dependence on the control amplitude b_0. The value of γ is chosen as $\gamma=9$, 10.5, 10.6, and 13 in panels (a), (b), (c), and (d), respectively. It can be seen that the Pyragas orbit is stabilized by a transcritical bifurcation $\mathbf{T}_1$. As the value of γ increases, a pair of a stable and an unstable orbit, generated by a fold bifurcation $\mathbf{F}_1$, approaches the minus branch [see Fig. 4(a)]. On this branch, fold bifurcations ($\mathbf{F}_2$ and $\mathbf{F}_3$) occur as shown in Fig. 4(b). At $\gamma=10.6$, the fold points of $\mathbf{F}_1$ and $\mathbf{F}_2$ touch in a transcritical bifurcation $\mathbf{T}_2$ and annihilate [see Figs. 4(c) and 4(d)]. Thus, for a further increase of γ, one is left with the stable minus branch and the unstable orbit, which was generated at the fold bifurcation $\mathbf{F}_3$. In all panels the radius of the Pyragas orbit is not changed by the control. The radius of the minus branch, however, is altered because the delay time does not match the orbit period.

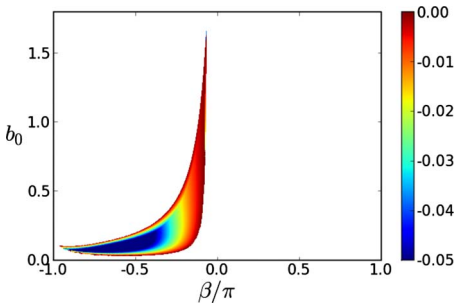

FIG. 5. (Color online) Domain of stability of the Pyragas orbit. The gray scale (color code) shows only negative values of the largest real part of the Floquet exponents. Parameters: $\omega_0=1$, $\lambda=0.0001$, $\gamma=0.1$ (cf. also Fig. 11).

Figure 5 shows the region in the (β,b_0) plane where the Pyragas orbit is stable for a set of parameters. The gray scale (color code) shows only negative values of the largest real part of the Floquet exponents. One can see that the orbit is most stable for feedback phases $\beta\approx-\pi/2$, which agrees with the previous analytic results for small λ. The picture was obtained by linear stability analysis of Eqs. (18) and (19) and the numerical solution of the transcendental eigenvalue problem for the Floquet exponents (see Appendix B).

III. APPLICATION TO ALL-OPTICAL CONTROL OF SEMICONDUCTOR LASERS

Lasers in stationary states emit rotating waves. A first step toward various instabilities is often the destruction of these states or the creation of additional ones in fold bifurcations. This happens generically when a laser is coupled to other lasers or to external cavities [9]. In what follows, we investigate to what extent the results of Sec. II can be transferred to lasers in such situations. In particular, we consider an integrated tandem laser (ITL), which is integrating two single-mode lasers coupled by a passive waveguide section on a monolithic semiconductor chip (cf. Fig. 6). Devices of this type are applied in ultrafast optical communication [10,11]. Depending on pump currents, they exhibit different types of bifurcations and dynamics at tens of GHz, and THz are within reach [12,13]. Control on those ultrashort picosec-

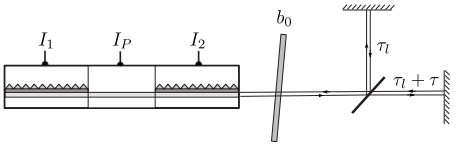

FIG. 6. Schematic diagram for all-optical delayed feedback control. The emission from one facet of an integrated tandem laser is injected into a Michelson interferometer. Two reflected waves return from there with different delays τ_l and $\tau_l+\tau$. Their superposition is reinjected into the device and serves as a control force. The amplitude b_0 of the control is adjusted by a neutral density filter. The control phase β rotates by 2π when changing the pathway between laser and interferometer by one wavelength.

ond time scales can be performed only in the optical domain, which profits from the ultimately high speed of light. Two schemes have been proposed: optical feedback either from a Michelson interferometer [14] or from a Fabry-Perot interferometer [15]. Experimental all-optical time-delayed feedback control has been developed only recently, exploiting optical feedback from a Fabry-Perot interferometer to stabilize unstable steady states of an ITL close to a Hopf bifurcation [7]. In the present work we consider the Michelson configuration [14], which is the optical version of the Pyragas method. The corresponding scheme is sketched in Fig. 6.

A. System without control

In order to describe the dynamics, we use the coupled rate-equations model for ITL lasers in dimensionless form [16]

$$\dot{E}_1 = i\delta E_1 + (1 + i\alpha)N_1 E_1 + \eta e^{-i\varphi} E_2, \tag{20}$$

$$\dot{N}_1 = \varepsilon[J - N_1 - (1 + 2N_1)|E_1|^2], \tag{21}$$

$$\dot{E}_2 = (1 + i\alpha)N_2 E_2 + \eta e^{-i\varphi} E_1 + E_b(t), \tag{22}$$

$$\dot{N}_2 = \varepsilon[J - N_2 - (1 + 2N_2)|E_2|^2], \tag{23}$$

extended by the control term $E_b(t)$, which is disregarded for the moment and will be specified later [in Eq. (25)]. The complex amplitudes $E_{1,2}$ and the real quantities $N_{1,2}$ represent the optical fields and the carrier densities in the two single-mode distributed feedback (DFB) lasers, respectively; δ accounts for the frequency detuning between them; J stands for pumping currents; η and φ characterize the coupling rate and the optical phase shift, respectively, between the two DFB sections; α denotes the linewidth-enhancement factor characterizing the amplitude-phase coupling typical for semiconductor lasers; $\varepsilon = \tau_p/\tau_n$ is the ratio between photon (τ_p) and carrier (τ_n) lifetimes; and τ_p serves as a unit of time. It is important to know that $E_{1,2}(t)$ represents slowly varying amplitudes. The full temporal variation of the optical fields is

$$\mathcal{E}_{1,2}(t) = E_{1,2}(t)e^{i\omega_0 t}, \tag{24}$$

with the optical reference frequency ω_0 playing the role of the corresponding quantity ω_0 in Sec. II. In the present formulation, ω_0 is the optical frequency of laser 2 in its unperturbed ($\eta = E_b = 0$) stationary state $N_2 = 0$, $E_2 = \text{const}$. At communication wavelengths around $\lambda = 1.55$ μm, we have $\omega_0 \approx 10^{15}$ s^{-1}. The corresponding dimensionless value is 50 000 when assuming $\tau_p = 5$ ps. The dynamics of $E(t)$ and $N(t)$ takes place on time scales which are more than three orders of magnitude slower.

System (20)–(23) without control, i.e., $E_b = 0$, was considered in detail in Ref. [16]. Rotational symmetry manifests itself by the invariance with respect to the transformation $(E_1, E_2) \mapsto (e^{i\theta}E_1, e^{i\theta}E_2)$ for any $e^{i\theta}$ in the unit circle S^1. This causes periodic solutions in the form of rotating waves $(E_1, N_1, E_2, N_2) = (a_1 e^{i\omega t}, n_1, a_2 e^{i\omega t}, n_2)$ with real constants

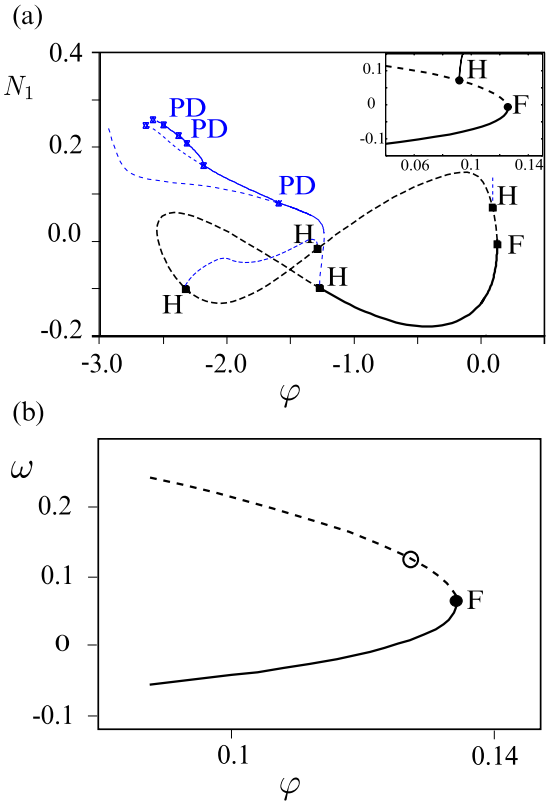

FIG. 7. (Color online) (a) Bifurcation diagram for the system (20)–(23) without control; i.e., $b_0 = 0$. Inset: a zoom close to the fold bifurcation F. Thick lines: rotating waves; thin lines: modulated waves (self-pulsations). Stable and unstable parts of the diagram are shown by solid lines and dashed lines, respectively. H: Hopf bifurcation; PD: periodic doubling of self-pulsations. (b) Frequencies of rotating waves close to the fold bifurcation of panel (a). Open circle: exemplary target state for stabilization. Other parameters are $\varepsilon = 0.03$, $J = 1$, $\eta = 0.2$, $\delta = 0.3$, and $\alpha = 2$.

ω, n_1, n_2 and complex constants a_1 and a_2. When varying the phase φ of the internal coupling between the two DFB lasers, the rotating waves lose stability either in a Hopf bifurcation or in a fold bifurcation as shown in a typical bifurcation diagram presented in Fig. 7. The Hopf bifurcation gives rise to periodically modulated waves, called self-pulsations, which will not be considered furthermore. In the present context, we consider the problem of stabilization of unstable rotating waves close to the fold F. The frequencies ω of rotating waves near F are drawn in panel (b). They increase when moving up through F in concordance with the scenario $\gamma > 0$ considered in Sec. II. Thus, we can expect that the stabilization of the unstable branch by Pyragas-type feedback should be possible.

B. Optical control force

Under which conditions does optical feedback from a Michelson interferometer give rise to a Pyragas-type control term $E_b(t)$? Generally, E_b is proportional to the slowly varying amplitude of the light fed back from the interferometer, which in turn is the sum of two partial waves, each one reflected from a different mirror. Accordingly,

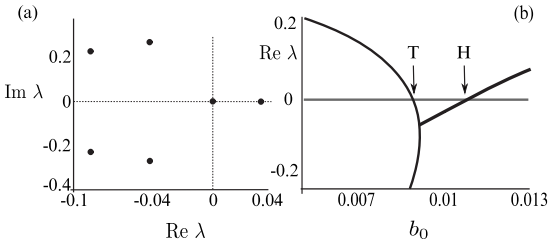

FIG. 8. (a) Floquet exponents of the uncontrolled target state. (b) Real part of leading Floquet exponents of the target state as a function of b_0 for $\beta=0$. T denotes transcritical, and H denotes Hopf bifurcations, respectively. Parameters are $\varepsilon=0.03$, $J=1$, $\eta=0.2$, $\delta=0.3$, $\alpha=2$, $\omega=0.1109$, $\varphi=0.1267$, $\tau_l=8$, $\tau=12$, and $\psi=\omega\tau$.

$$E_b(t) = b_0 e^{i\beta}[e^{i\psi}E_2(t-\tau_l-\tau) - E_2(t-\tau_l)]. \qquad (25)$$

τ_l and $\tau_l+\tau$ are the travel times of light on the two pathways. τ corresponds to the control delay time of Eq. (6) and τ_l is an additional latency, which unavoidably occurs in real systems. The two optical phase shifts $\beta=-(\omega_0\tau_l+\pi)$ and $\psi=-(\omega_0\tau+\pi)$ are associated with the respective delays. They are the impact of the fast optical phase rotation (24) on the slow amplitudes of delayed light. The π is added in both cases to obtain consistency with the choice of signs in Sec. II. Further possible phase shifts, e.g., from reflections at mirrors, may also be incorporated this way. Both phases are tunable by subwavelength changes of the respective optical pathways which have no effect on the slow amplitudes. Thus, they are regarded as independent parameters. The feedback amplitude b_0 contains all attenuations on the respective round trips. Note that equal attenuation on both pathways is assumed, otherwise destructive interference remains incomplete and noninvasiveness is not achievable. Noninvasiveness also requires proper adjustment of phase ψ. Indeed, when the target state is a rotating wave $E_2(t)=a_2e^{i\omega t}$, the control term vanishes for $e^{i(\psi-\omega\tau)}=1$. This is the well-known condition for destructive interference: nothing is reflected if the two returning partial waves have opposite amplitudes. Control phase β and amplitude b_0 are free parameters playing the same role as the corresponding quantities in Sec. II.

C. Stabilization of rotating waves

Now we study stabilization of rotating waves on the unstable branch close to the fold bifurcation in Fig. 7. We fix the delays of the control term as $\tau_l=8$ and $\tau=12$, corresponding to about 40 and 60 ps, respectively, which are accessible in experiment [7]. These parameters are not critical; other values of the same order yield similar results.

Exemplarily, we address the unstable state $\omega=0.1109$ at $\varphi=0.1267$ [open circle in Fig. 7(b)], which without control indeed has a single positive Floquet exponent [20] [Fig. 8(a)]. With control ($b_0>0$), this target state itself does not get light back and keeps unchanged by setting $\psi=\omega\tau=1.3308$. Only deviations from it cause a nonvanishing feedback, which in fact modifies its stability. These effects and the resulting bifurcations have been calculated by applying the software package DDE-BIFTOOL [17] to the delay-differential system (20)–(23). Now the leading Floquet exponents change with b_0 is plotted in Fig. 8(b) for $\beta=0$. With increasing b_0, the unstable real Floquet exponent decreases and becomes negative in point T. This stabilization is due to a transcritical bifurcation T, as predicted in Sec. II. In terms of the Floquet multipliers this indicates that an unstable multiplier crosses the unit circle at 1. With a further increase of the control parameter b_0, first, two branches of eigenvalues with negative real parts coalesce and then a destabilization takes place, when the two complex conjugate eigenvalues become unstable; i.e., a Hopf bifurcation to self-pulsating solutions occurs in point H in Fig. 8(b). The zero line in Fig. 8(b) corresponds to the trivial Floquet exponent, which occurs due to the symmetry and does not influence the stability.

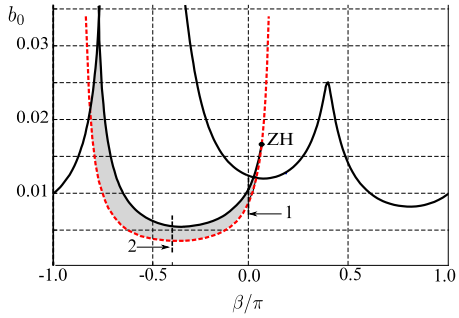

FIG. 9. (Color online) Two-dimensional bifurcation diagram of the target state with respect to the control parameters b_0 and β. Black solid line: Hopf bifurcation. Above this line the laser emits self-pulsations. Red dashed line: transcritical bifurcation. Below this line, the target state is unstable. The gray area denotes the stability region. *ZH* is the zero-Hopf bifurcation of codimension two. Line 1 corresponds to the parameter path along which the eigenvalues are computed in Fig. 8(b). Line 2 corresponds to the parameter changes in Fig. 10. Other parameters are as in Fig. 8.

A two-parameter bifurcation diagram of the same rotating wave in the plane (β,b_0) is shown in Fig. 9. The stability region is bounded by the Hopf and transcritical bifurcations mentioned before. The role of these bifurcations is as predicted by the generic model in Sec. II and also, the shape is similar to that of Fig. 5. It is interesting to compare this bifurcation diagram to other known cases of all-optical control. A simple single-mode laser exposed to noninvasive control of type (25) changes stability similarly by transcritical and Hopf bifurcations [18]—only the laser is destabilized but not stabilized. In case of rotating waves beyond a Hopf bifurcation in an ITL laser, the domains of control are also bounded by Hopf and transcritical bifurcations but with different ordering: inverse Hopf defines the lower bound whereas the upper bound is partly transcritical [7,19]. Quantitatively, the vertical extension of the present control domain near a fold bifurcation is, however, small compared to the latter case. Thus, a possible experimental stabilization near folds will probably require a more precise adjustment of control amplitude b_0 compared to Refs. [7,19].

To investigate the influence of the control on the environment of the target state, we recalculated the bifurcation diagram of Fig. 7(b) with control parameters on the vertical line 2 in Fig. 9. The resulting branches of rotating waves are compared to those of the uncontrolled device in Fig. 10. Panel (a) exemplifies the particular case $b_0=0.005$. Apart

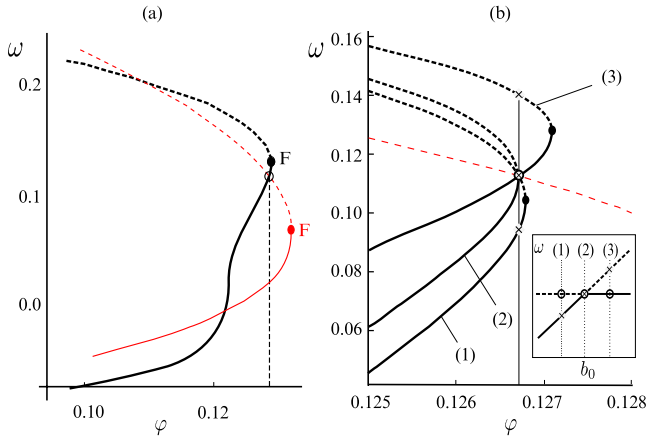

FIG. 10. (Color online) Branches of stable (solid) and unstable (dashed) rotating waves without control (thin) and with control (thick). F: fold bifurcation. Vertical line: $\varphi=0.1267$ of the chosen target state. Open circle: target state. (a) $b_0=0.005$. (b) (1) $b_0=0.0030$ below, (2) $b_0=0.0035$ at, and (3) $b_0=0.0050$ above the control threshold. Inset: relation to the transcritical bifurcation. Parameters are as in Fig. 9 and $\beta=-0.408\pi$, $\psi=1.3308$.

from the target state (open circle), which keeps unchanged on purpose, the feedback is invasive and changes the laser state. Due to the smallness of b_0, the modifications are minor [note the small zoom compared to the full bifurcation diagram Fig. 9(a)]. The fold bifurcation is preserved and shifted slightly above the target state. As a consequence, the target is now on the stable branch. The stabilization transition happens when the fold bifurcation crosses the unstable branch of the uncontrolled system exactly in the target state. The target is the upper of the two states with $\varphi=0.1267$; it is unstable for smaller b_0 (curve 1) and stable for larger b_0 (curve 3). Both states cross in a transcritical bifurcation (inset), in agreement with the results of Sec. II.

IV. CONCLUSIONS

We have shown that, contrary to common belief, unstable periodic states with an odd number of real Floquet multipliers greater than unity, here created by a fold bifurcation, can indeed be stabilized by time-delayed feedback control. As a promising all-optical realization we propose an integrated semiconductor tandem laser combined with a Michelson interferometer.

Our analysis is complementary to the previous publications on this topic [4–6], which have been devoted to the stabilization of unstable periodic orbits close to a subcritical Hopf bifurcation. The approaches which have been used in the above papers are specifically based on the normal form at the subcritical Hopf bifurcation and cannot be simply transferred to the fold case. The common point in both scenarios of stabilization is the appearance of a transcritical bifurcation resulting from the two basic assumptions: vanishing control term for the Pyragas orbit, and the existence of one unstable real positive Floquet multiplier.

Note that one can perturb Eqs. (6) or Eqs. (20)–(23), such that the S^1 symmetry is broken. In this case the stable (unstable) rotating waves will be perturbed into stable (unstable) periodic solutions, respectively, which will no longer have the form of rotating waves. Thus, by rigorous perturbative arguments, our paper refutes the odd-number limitation also, for periodic solutions which are not rotating waves. On the other hand, in nonautonomous systems the odd-number limitation may still hold [5].

ACKNOWLEDGMENTS

We gratefully acknowledge the support of DFG in the framework of Sfb555.

APPENDIX A

In this Appendix, we derive conditions (12) and (13) at which the transcritical bifurcation in system (6) occurs. To derive Eq. (12) we could proceed by brute force: linearize the control system (6) along the Pyragas branch, in polar coordinates; derive the characteristic equation in a corotating coordinate frame; eliminate the trivial zero characteristic root; and determine $\tau=\tau_c$, $r=r_c$, and $b_0=b_c$ such that a nontrivial zero characteristic root remains. Instead, we will proceed locally in a two-dimensional center manifold of the fold, following the arguments in Just *et al.* [5], as given in Appendix B below. Any periodic solution in the center manifold of Eq. (6) is a rotating wave $z(t)=re^{i\omega t}$.

Hence, let us compute the rotating waves of the system (6), globally. Substituting $z(t)=re^{i\omega t}$ into Eq. (6) and decomposing into real and imaginary parts, we obtain

$$0 = g(\lambda, r^2) + 2b_0 \sin\frac{\omega\tau}{2}\sin\left(\beta - \frac{\omega\tau}{2}\right), \tag{A1}$$

$$\omega = h(\lambda, r^2) - 2b_0 \sin\frac{\omega\tau}{2}\cos\left(\beta - \frac{\omega\tau}{2}\right). \tag{A2}$$

With $\varepsilon=r^2-1$ and our choices (4) for g and h, these equations become

$$0 = \varepsilon^2 - \lambda(\tau) + 2b_0 \sin\frac{\omega\tau}{2}\sin\left(\beta - \frac{\omega\tau}{2}\right), \tag{A3}$$

$$\omega = \gamma\varepsilon + \omega_0 - 2b_0 \sin\frac{\omega\tau}{2}\cos\left(\beta - \frac{\omega\tau}{2}\right). \tag{A4}$$

For small enough b_0, we can solve Eq. (A4) for $\omega=\omega(\varepsilon)$ and insert into Eq. (A3),

$$0 = G(\tau, \varepsilon). \tag{A5}$$

Here $G(\tau,\varepsilon)$ abbreviates the right-hand side of Eq. (A3) with $\omega=\omega(\varepsilon)$ substituted for ω. The condition for a transcritical bifurcation in the system with control then reads

$$0 = \frac{\partial}{\partial\varepsilon}G(\tau_c, \varepsilon), \tag{A6}$$

in addition to Eq. (A5). It simplifies matters significantly that this calculation has to be performed along the Pyragas

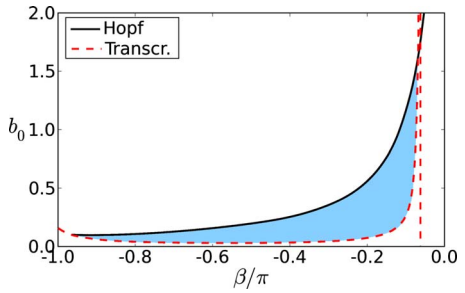

FIG. 11. (Color online) Plot of transcritical (dashed) and Hopf bifurcation line (solid) and the domain of stability (shaded region) in the (β, b_0) plane. Parameters are as in Fig. 5.

branch only, where $\omega\tau = 2\pi\tau/T = 2\pi k$; see Eq. (7). Therefore Eq. (A6) becomes

$$0 = \frac{\partial}{\partial\varepsilon} G(\tau_c, \varepsilon) = 2\varepsilon + b_0\tau_c \cos k\pi \sin(\beta - k\pi)\omega'(\varepsilon)$$
$$= 2\varepsilon + b_0\tau_c\omega'(\varepsilon)\sin\beta. \tag{A7}$$

To obtain the derivative ω' of ω, with respect to ε, we have to differentiate Eq. (A4) implicitly, at $\omega\tau = 2k\pi$.

$$\omega' = \gamma - b_0\tau\omega' \cos\beta.$$

Solving for ω' for small b_0 yields

$$\omega' = \frac{\gamma}{1 + b_0\tau\cos\beta} = \frac{\gamma}{1 + b_0\frac{2k\pi}{\omega_0 + \gamma\varepsilon}\cos\beta}. \tag{A8}$$

Here we have used $\omega\tau = 2k\pi$ and $\omega = \omega_0 + \gamma\varepsilon$. Plugging Eq. (A8) into Eq. (A7), the control amplitude b_0 enters linearly, and we obtain

$$0 = \varepsilon(\omega_0 + \gamma\varepsilon)\left(1 + b_0\frac{2k\pi}{\omega_0 + \gamma\varepsilon}\cos\beta\right) + b_0 k\pi\gamma\sin\beta$$
$$= \varepsilon(\omega_0 + \gamma\varepsilon + b_0 2k\pi\cos\beta) + b_0 k\pi\gamma\sin\beta. \tag{A9}$$

Solving for b_0, we obtain the required expression (12) for the value of the control amplitude, at which the transcritical bifurcation occurs.

The equivalent condition (13) follows from Eq. (12) by straightforward substitution of Eq. (8) and $-\sqrt{\lambda} = r^2 - 1 = \varepsilon$.

APPENDIX B

In this Appendix we perform a linear stability analysis of the Pyragas orbit. Linearizing Eqs. (18) and (19) around the Pyragas orbit according to $z(t) = (r + \delta r)\exp(i\omega t + i\delta\varphi)$, we find

$$\frac{d}{dt}\begin{pmatrix}\delta r(t)\\ \delta\varphi(t)\end{pmatrix} = \begin{bmatrix}\partial_r g r + g - b_0\cos\beta & r b_0\sin(\beta - \omega\tau)\\ \partial_r h - b_0\sin(\beta - \omega\tau)\frac{1}{r} & -b_0\cos(\beta - \omega\tau)\end{bmatrix}\begin{pmatrix}\delta r(t)\\ \delta\varphi(t)\end{pmatrix} + \begin{bmatrix}b_0\cos(\beta - \omega\tau) & -r b_0\sin(\beta - \omega\tau)\\ b_0\sin(\beta - \omega\tau)/r & b_0\cos(\beta - \omega\tau)\end{bmatrix}\begin{pmatrix}\delta r(t - \tau)\\ \delta\varphi(t - \tau)\end{pmatrix}.$$

The delay time τ matches the period of the Pyragas orbit and we thus have

$$\omega\tau = 2\pi k.$$

Using the exponential ansatz $(\delta r(t), \delta\varphi(t)) \propto \exp\Lambda t$ gives a transcendental equation for the Floquet exponents Λ as follows:

$$\det\begin{bmatrix}4(r^2 - 1)r^2 + (r^2 - 1)^2 - \lambda - \Lambda - b_0\cos\beta(1 - e^{-\Lambda\tau}) & r b_0\sin\beta(1 - e^{-\Lambda\tau})\\ 2\gamma r - (b_0/r)\sin\beta(1 - e^{-\Lambda\tau}) & -\Lambda - b_0\cos\beta(1 - e^{-\Lambda\tau})\end{bmatrix} = 0. \tag{B1}$$

This equation was numerically solved to obtain Fig. 5.

One can find the Hopf bifurcation of the Pyragas orbit in a semianalytic way by inserting $\Lambda = i\Omega$ into Eq. (B1) and separating the equation into real and imaginary parts as follows:

$$\text{Real:}\quad 0 = -\Omega^2 - 2\Omega b_0\cos\beta\sin(\Omega\tau) - b_0(cr\sin\beta + a\cos\beta)[1 - \cos(\Omega\tau)] - b_0^2 2[1 - \cos(\Omega\tau)]\cos(\Omega\tau), \tag{B2}$$

$$\text{Imag:}\quad 0 = -a\Omega + 2\Omega b_0\cos\beta[1 - \cos(\Omega\tau)] - b_0(cr\sin\beta + a\cos\beta)\sin(\Omega\tau) + b_0^2 2[1 - \cos(\Omega\tau)]\sin(\Omega\tau). \tag{B3}$$

We can now use Ω as a parameter and solve the two equations for β and b_0 at each Ω. The resulting Hopf curve and the transcritical bifurcation curve (12) then form the boundary of the control domain (Fig. 11).

[1] *Handbook of Chaos Control*, 2nd ed., edited by E. Schöll and H. G. Schuster (Wiley-VCH, Weinheim, 2008).
[2] E. Ott, C. Grebogi, and J. A. Yorke, Phys. Rev. Lett. **64**, 1196 (1990).
[3] K. Pyragas, Phys. Lett. A **170**, 421 (1992).
[4] B. Fiedler, V. Flunkert, M. Georgi, P. Hövel, and E. Schöll, Phys. Rev. Lett. **98**, 114101 (2007).
[5] W. Just, B. Fiedler, M. Georgi, V. Flunkert, P. Hövel, and E. Schöll, Phys. Rev. E **76**, 026210 (2007).
[6] C. M. Postlethwaite and M. Silber, Phys. Rev. E **76**, 056214 (2007).
[7] S. Schikora, P. Hövel, H.-J. Wünsche, E. Schöll, and F. Henneberger, Phys. Rev. Lett. **97**, 213902 (2006).
[8] Y. Kuznetsov, in *Elements of Applied Bifurcation Theory*, Applied Mathematical Sciences Vol. 112 (Springer-Verlag, Berlin, 1995).
[9] *Fundamental Issues of Nonlinear Laser Dynamics*, edited by B. Krauskopf and D. Lenstra, AIP Conf. Proc. No. 548 (AIP, New York, 2000).
[10] C. Bornholdt, J. Slovak, and B. Sartorius, Electron. Lett. **40**, 192 (2004).
[11] J. Slovak, C. Bornholdt, J. Kreissl, S. Bauer, M. Biletzke, M. Schlak, and B. Sartorius, IEEE Photon. Technol. Lett. **18**, 844 (2006).
[12] Inwoong Kim, Cheolhwan Kim, Guifang Li, P. LiKamWa, and Jin Hong, IEEE Photon. Technol. Lett. **17**, 1295 (2005).
[13] M. Al-Mumin, C. Kim, I. Kim, N. Jaafar, and G. Li, Opt. Commun. **275**, 186 (2007).
[14] W. Lu and R. G. Harrison, Opt. Commun. **109**, 457 (1994).
[15] J. E. S. Socolar, D. W. Sukow, and D. J. Gauthier, Phys. Rev. E **50**, 3245 (1994).
[16] S. Yanchuk, K. R. Schneider, and L. Recke, Phys. Rev. E **69**, 056221 (2004).
[17] K. Engelborghs, T. Luzyanina, and G. Samaey, Technical Report No. TW 330, Katholieke Universiteit Leuven, 2001 (unpublished).
[18] V. Z. Tronciu, H. J. Wünsche, M. Wolfrum, and M. Radziunas, Phys. Rev. E **73**, 046205 (2006).
[19] *Handbook of Chaos Control*, 2nd ed., edited by E. Schöll and H. G. Schuster (Wiley-VCH, Weinheim, 2008), Chap. 21.
[20] Note that due to the rotational symmetry of the system, the rotating waves $(a_1 e^{i\omega t}, n_1, a_2 e^{i\omega t}, n_2)$ are usually transformed into the family of equilibria $(a_1 e^{i\theta}, n_1, a_2 e^{i\theta}, n_2)$, $0 \leq \theta < 2\pi$ in the rotating coordinate system. For these equilibria, it is meaningful to speak about their eigenvalues. These eigenvalues coincide with the Floquet exponents of the original time-periodic rotating waves. An additional zero eigenvalue of these equilibria appears due to the symmetry.